catalysts

MDPI

Article

The Catalytic Effect from Alkaline Elements on the Tar-Rich Coal Pyrolysis

Zhonghua Du and Wu Li *

Key Laboratory of Coalbed Methane Resource & Reservoir Formation Process, Ministry of Education, China University of Mining and Technology, Xuzhou 221008, China; du_zhonghua@cumt.edu.cn
* Correspondence: liwu@cumt.edu.cn

Abstract: Tar-rich coal has been widely concerned because of its high tar yield. Two kinds of tar-rich coals were studied by Thermogravimetric-Mass spectrometer-Fourier transform infrared (TG-MS-FTIR) to obtain the pyrolysis characteristics. TG-MS-FTIR was used to study the mass loss, gaseous compounds evolution, and functional group information of tar-rich coal during pyrolysis. Mass loss is mainly caused by water release and macromolecular decomposition. The results showed that there were two stages of mass loss in the pyrolysis process. In addition, the gas release signal detected by mass spectrometry is consistent with the functional group information detected by FTIR. The main gaseous products include H_2, H_2O, CO, CO_2, and CH_4. In addition, the effect of ash content on the pyrolysis of oil-rich coal and the catalytic effect of internal minerals on coal pyrolysis are also discussed, and the thermal pyrolysis characteristics of coke-rich oil coal are put forward. The results provide a new idea for the study of pyrolysis characteristics of tar-rich coal.

Keywords: tar-rich coal; pyrolysis; TG-MS-FTIR; catalysis

Citation: Du, Z.; Li, W. The Catalytic Effect from Alkaline Elements on the Tar-Rich Coal Pyrolysis. *Catalysts* **2022**, *12*, 376. https://doi.org/10.3390/catal12040376

Academic Editors: Baiqian Dai, Xiaojiang Wu and Lian Zhang

Received: 25 February 2022
Accepted: 22 March 2022
Published: 27 March 2022

1. Introduction

As a coal resource integrating kerosene and gas attributes, tar-rich coal has attracted the attention of scholars all over the world [1–4]. Coal with a low temperature (500–700 °C) tar yield of more than 7% and less than or equal to 12% is called tar-rich coal [5]. The excellence of oil-rich coal is mainly reflected in its hydrogen-rich structure, which can produce oil and gas by pyrolysis. Moreover, the tar yield after pyrolysis is high, and the semicoke produced by pyrolysis can become a substitute for anthracite and coking coal. Based on the advantages, tar-rich coal is considered to be an important way to increase oil and gas supply and realize clean and efficient utilization of coal resources.

The research on the pyrolysis behavior of coal has been proved to be significant for the efficient production and utilization of coal [6–9]. Under isolated air conditions, coal can generate oil, gases, and semicoke at low or medium temperatures [10]. Tar-rich coal makes it unique in terms of the yield of tar produced by pyrolysis. As is well-known, the pyrolysis behavior of coal is always of primary concern [11–14]. A large amount of literature focused on investigating the thermal behavior of tar-rich coal under different conditions to improve the yield of pyrolysis products. Jiang et al. investigated an integrated process of coal pyrolysis with steam reforming of propane (CP-SRP) to improve tar yield using Ni/Al_2O_3 as a reforming catalyst [15]. The results suggested that the CP-SRP and the integrated coal pyrolysis with steam reforming of methane (CP-SRM) or methane with a few propane (CP-SRMP) showed a higher tar yield. Yao et al. reported detailed research on the effects of ion-exchanged metal cations on the pyrolysis reactivity of Shendong demineralized coal (SD-coal) and the gasification performance of pyrolysis chars [16]. It was suggested that the char yields decreased, and the pyrolysis gas yields increased during the pyrolysis of metal ion-exchanged coals. The catalytic effect of different ion exchanges on the yield of pyrolysis products was different. Li et al. analyzed the characteristics of coal pyrolysis products at various temperatures using a drop tube furnace, and the composition of pyrolysis products

was characterized and discussed [17]. Results showed that pyrolysis was a dehydration upgrading process for lignite. The previous studies mainly focused on the pyrolysis law of different types, different ranks, and different particle sizes of coal [18–20]. However, the pyrolysis kinetics and pyrolysis product information of tar-coal are rarely reported.

Thermogravimetric-Mass spectrometer-Fourier transform infrared (TG-MS-FTIR) analyzer has been widely used in these processes because of its sensitivity. TG-MS-FTIR combined thermogravimetry, mass spectrometry, Fourier transform infrared spectroscopy, and computer system online analysis. This technique can provide useful information so as to investigate the pyrolysis reaction mechanism and analysis of thermal pyrolysis products [21,22]. In literature, there are some studies that include TG-MS-FTIR analysis for different kinds of coal [23–25]. Pan et al. analyzed the pyrolysis behavior and gas product information of four kinds of pulverized coal in different regions by TG-MS-FTIR. The results show that coal with a relatively low H/C ratio may lead to a relatively stronger thermal reaction [23]. Wang et al. studied the chemical composition and chemical structure of five coals in southern China by TG-MS-FTIR and analyzed the evolution process of pyrolysis gas products [24].

From the perspective of coal chemistry, the evolution behavior of inorganic minerals in coal has an obvious impact on the operating parameters and stability of the coal thermal conversion process. Coal pyrolysis is a key step and an important component of thermal transformation, in which minerals become important factors affecting the process and products of coal pyrolysis. Predecessors have compared the mineral composition, microcrystalline structure, surface morphology, pyrolysis characteristics, and product changes of coal before and after complete deashing to study the effect of minerals on coal pyrolysis [26–31].

Coal is a heterogeneous mixture of complex organic macromolecules and different amounts of inorganic minerals. Coal pyrolysis usually refers to the reflection of the organic structure of coal at high temperatures, which is inevitably affected by the type and content of minerals in coal. However, due to the differences in the coal forming environment and research methods, there are great differences in the evaluation of the impact of internal minerals on coal pyrolysis characteristics by different researchers. Liu et al. Found that the internal minerals in coal have no significant effect on the pyrolysis reaction activity and kinetic parameters of coal. When calcium oxide, potassium carbonate, and alumina are added, the inorganic minerals have a positive effect on the pyrolysis reaction activity of coal, which is related to the temperature and the type of coal [32]. Howard found that calcium-containing minerals can reduce the yield of hydrocarbons in the nitrogen atmosphere, and clay minerals have little effect on coal pyrolysis [33]. The research of Ahamad et al. also shows that the internal minerals of coal will affect the formation of hydrocarbons during coal pyrolysis [34].

In this paper, the TG-MS-FTIR technique was first used to analyze the pyrolysis behavior and gaseous compounds in different stages during the pyrolysis of tar-rich coal. Combining the information of thermogravimetric curves, thermal pyrolysis products, and functional group, the thermal pyrolysis mechanism of tar-rich coal was proposed. The thermal pyrolysis behavior information can provide theoretical support for the development and utilization of tar-rich coal.

2. Results and Discussion

2.1. The Thermal Characterisation for Coal Pyrolysis

The TG and DTG curves of the coal samples at 10 °C/min are shown in Figure 1. Evidently, the pyrolysis behavior of the sample occurred at temperatures higher than 400 °C, and the decomposition reaction continued as the temperature was increased. As shown in Figure 1, the DTG curve was asymmetric and could obviously be divided into multiple steps [35]. Therefore, PeakFit software was used to separate the overlapping peaks by adopting the Gaussian multipeak fitting method.

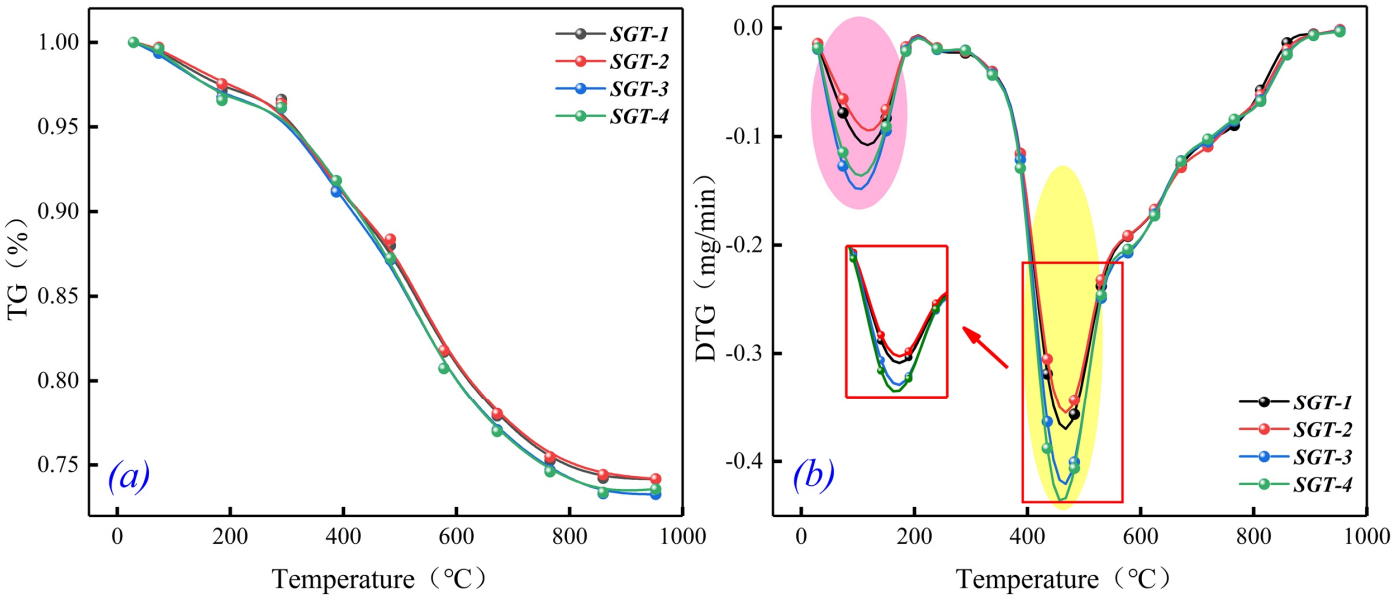

Figure 1. TG and DTG curves of coal samples ((**a**): TG curves, (**b**): DTG curves).

The pyrolysis evolution curves of samples can be divided into three stages in regard to temperature (Figure 2). The first stage is the drying and degassing stage, which ranges from room temperature to 350 °C. This stage was mainly caused by the volatilization of coal moisture (surface water and pore water), methane, and carbon dioxide adsorbed on the surface [36,37]. The temperature range of the second stage is 350–550 °C, which is a severe pyrolysis stage. The depolymerization and decomposition of coal mainly occurred at this stage, resulting in a significant increase in the weight loss of coal samples. With the softening of coal particles, semicoke began to form, and pyrolysis water, pyrolysis gas, and pyrolysis oil were separated. In the third stage, tar production began to decrease, hydrogen gas generation increased gradually, and aromatic nuclei of coal increased, which were arranged regularly and had better structure [38].

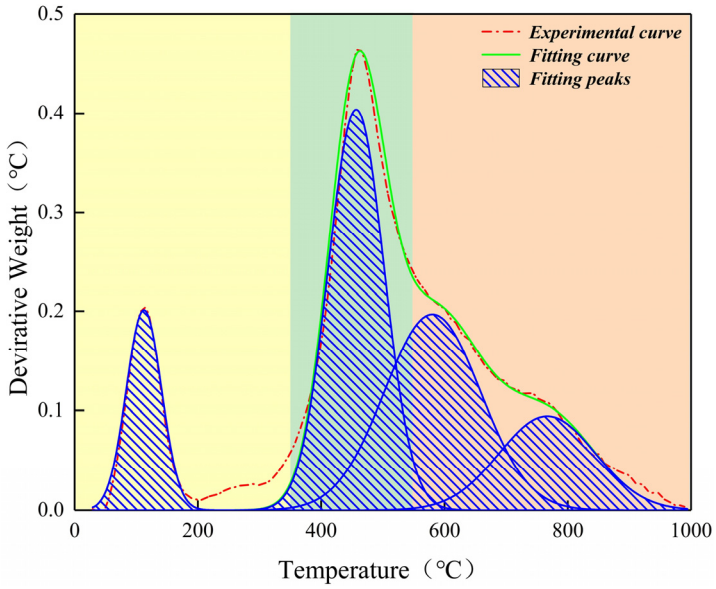

Figure 2. Peak fitting of DTG curve.

It can be seen from Figure 1 that the slopes of the four samples are roughly the same, which means that the decomposition rates of the four samples are the same under the same conditions. The DTG curves display that the samples experienced two weight losses during pyrolysis. The first weight loss was due to the evaporation of water in the sample [39]. The second weight loss was caused by the thermal decomposition of coal samples. The DTG curve fluctuated around 700 °C, mainly due to the decomposition of minerals in coal [40]. DTG curves of SGT-3 and SGT-4 were significantly different from other samples. The main reason was that the yield of volatile matter in SGT-3 and SGT-4 coal samples was higher than that of other coal samples. During this period, the devolatilization reaction mainly occurred in coal samples, including the depolymerization of macromolecules, through weak bridge bond and the removal of fatty side chain-cracking reactions in macromolecular structure, which led to the weight loss rate of coal samples higher than other coal samples [41].

Table 1 shows several special data of samples during pyrolysis. The temperatures of maximum weight loss of four samples were approximately the same. Besides, the maximum rates of weight loss of SGT-3 and SGT-4 were higher than other samples. The final weight loss was maintained at 26~28%.

Table 1. Summary of TG and DTG results.

Sample	T_{max}	$(dw/d\tau)_{max}$	W_{loss}
	°C	%/min	%
SGT-1	460.07	0.427	25.11
SGT-2	460.03	0.387	25.48
SGT-3	460.81	0.462	26.45
SGT-4	460.99	0.478	26.01

T_{max} is the temperature of maximum weight loss; $(dw/d\tau)_{max}$ is the maximum rate of weight loss; W_{loss} is the final weight loss.

2.2. The Gas Composition for Pyrolysis

Generally, the breaking of bridge bonds between aromatic rings, the disappearance of heteroatom functional groups, and the ring breaking of macromolecular networks will occur in the process of coal pyrolysis [42]. These reactions result in the production of gases and tar. Gas compounds can be collected by mass spectrometry.

The generation curves of CH_4 are shown in Figure 3. CH_4 is the main gaseous hydrocarbon product in the pyrolysis process [43]. From Figure 3, it can be seen that the main temperature range of methane generated was 400~900 °C. With the increase in temperature, the release rate of CH_4 increased first and was then reduced, reaching a peak at near 550 °C. In the low-temperature stage, CH_4 mainly came from the breaking of the C–C bond in aliphatic chains, whereas the formation of CH_4 at higher temperatures was due to the cleavage of stronger bonds [44].

CO_2 appeared at nearly 100 °C and reached its peak at about 500 °C (See Figure 4). Then, with the increase in temperature, the release rate of CO_2 began to come down. According to previous articles [45–47], the sources of CO_2 included carbon dioxide adsorbed in coal, decomposition of carbonate, and fracture of oxygen-containing functional groups. The formation of CO_2 in the early stage was related to the decomposition of the carboxyl group, while the latter was mainly the decomposition of ether structures and oxygen-bearing heterocycles.

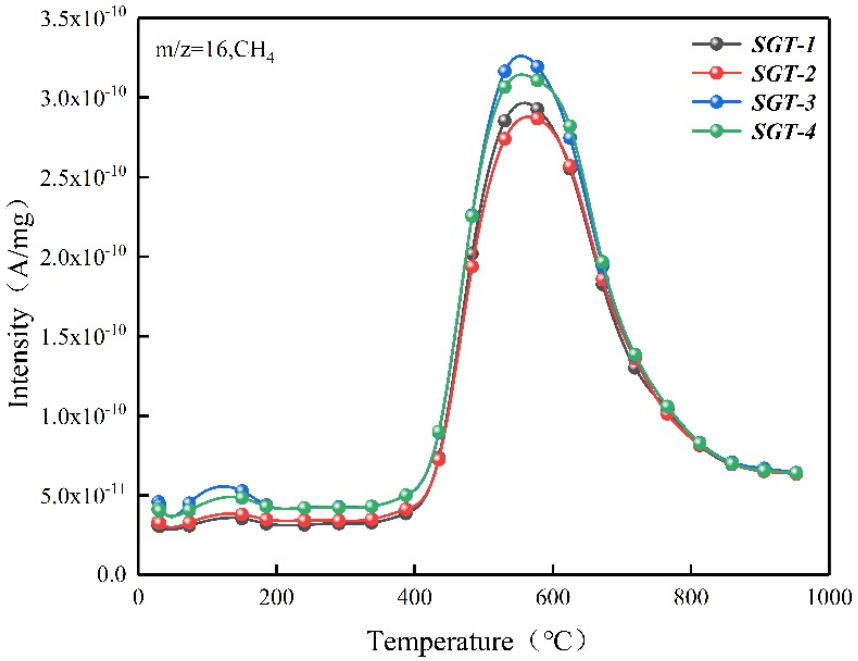

Figure 3. Evolution curves of CH_4.

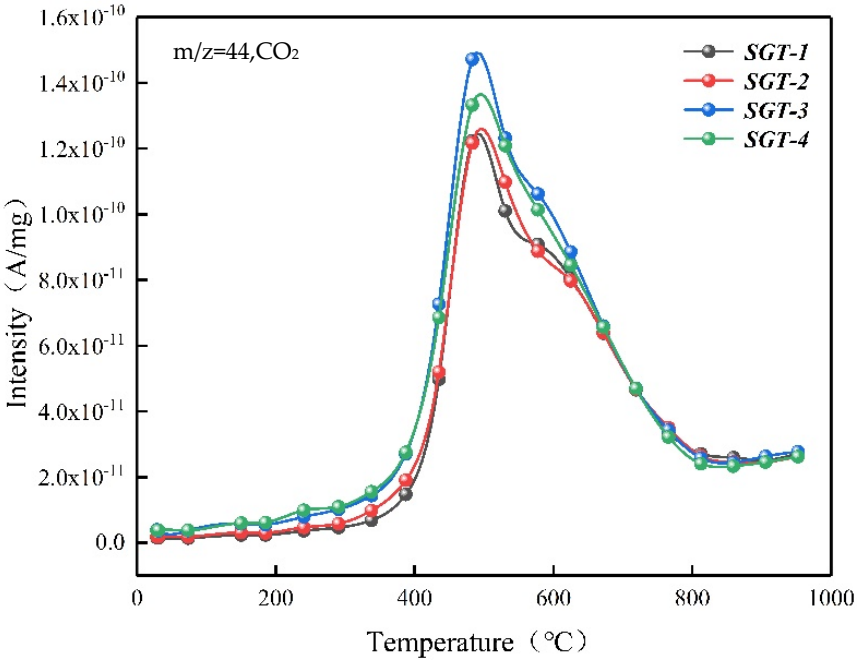

Figure 4. Evolution curves of CO_2.

From Figure 5, it can be seen that there are two main peaks in the evolution curves of H_2O. H_2O appeared at about 50 °C. With the temperature increased, the yield of H_2O went up and reached the first peak at nearly 150 °C and another one at about 540 °C. The temperature range of the first peak was from 70 °C to 200 °C. At this stage, the H_2O mainly came from the sample [48]. The other peak temperature range was about 400~800 °C. The release of water in the high-temperature section was mainly due to the decomposition of oxygen-containing functional groups [49].

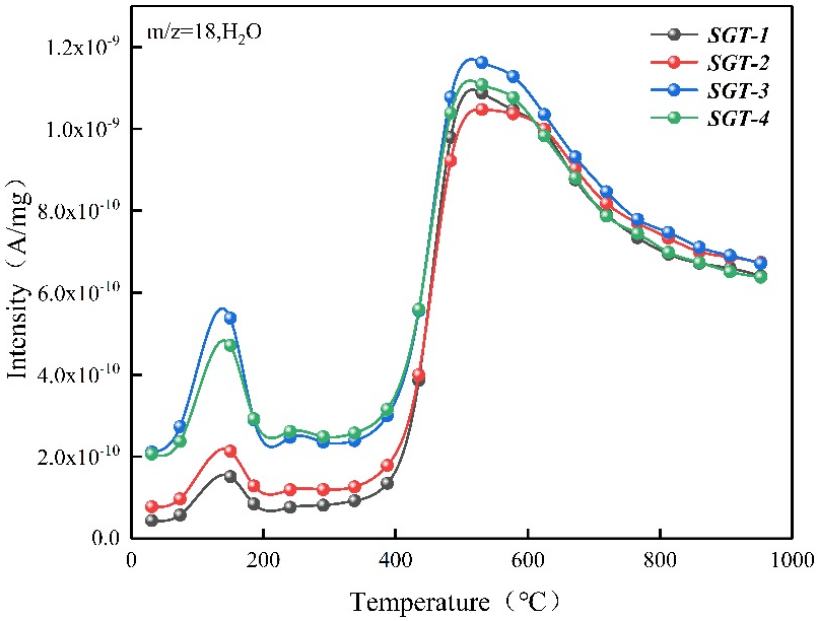

Figure 5. Evolution curves of H_2O.

Compared with other gases, the evolution of CO is more complex, and there is no obvious downward trend before 1000 °C (See Figure 6). At about 450 °C, the release rate of CO increased sharply, mainly due to the decomposition of the carbonyl group. At nearly 780 °C, the evolution curve of CO fluctuated again, which might be related to the decomposition of phenolic groups [50]. Actually, there is a process of mutual transformation between CO_2 and CO. CO_2 can decompose into CO and O_2, while CO can also be produced by the Boudouard reaction [51,52].

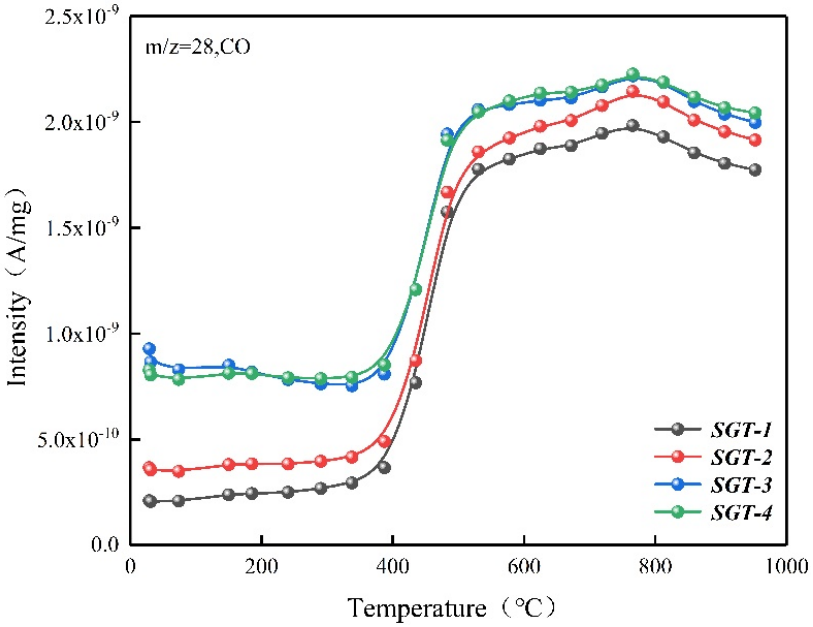

Figure 6. Evolution curves of CO.

H_2 was mainly generated from 400 °C to 1000 °C and reached a peak at about 770 °C (See Figure 7). Before 400 °C, the generation of H_2 related to the degradation of the hydrogen-rich matrix. At about 780 °C, the increase in H_2 release rate was due to the condensation of aromatic and hydroaromatic structures [53].

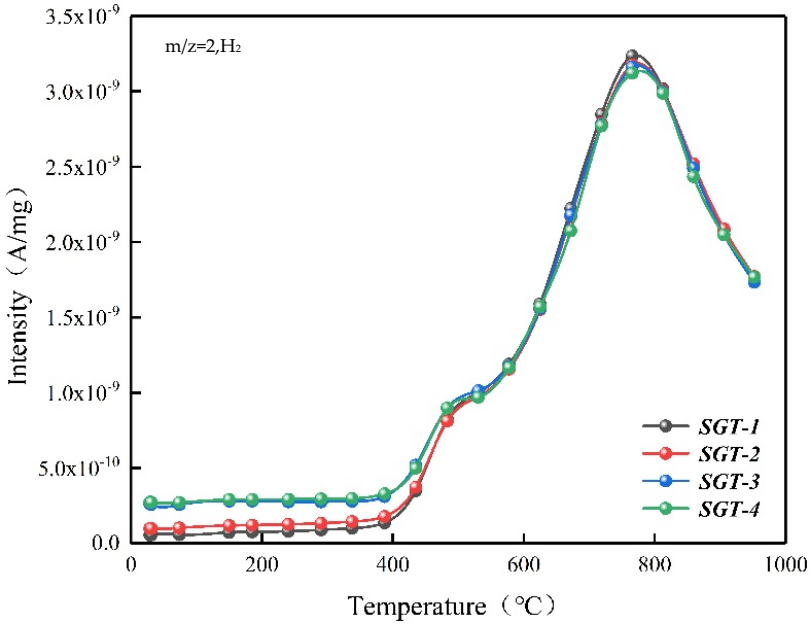

Figure 7. Evolution curves of H_2.

2.3. The Evolution of Carbon Compounds during Pyrolysis

FTIR technology can be used to capture the volatile products of coal pyrolysis on line. The change of absorption peak of the infrared spectrum can indirectly reflect the generation law of gas species and relative yield [54,55]. The reaction and volatile species in the pyrolysis process mainly depend on the amount of oxygen-containing functional groups, aromatic rings, and aliphatic branched chains [56,57].

The 3D FTIR diagram of coal thermal pyrolysis with a heating rate of 10 °C/min is shown in Figure 8. The significant infrared absorption bands with high absorbance at 2350 cm^{-1} and 1530 cm^{-1} are distinctly noticed. In order to further understand the differences of gaseous products, two-dimensional infrared spectra of volatile products at different temperatures are shown in Figure 9. FTIR with the spectral range of 4000–400 cm^{-1} was involved. The characteristic bands at 3850–3550 cm^{-1} and 1800–1500 cm^{-1} were proved to be H_2O [58,59]. In particular, the bands at 1500–1800 cm^{-1} included not only H_2O but also NH_3 (1800–1450 cm^{-1}), NO_2 (1700–1500 cm^{-1}), and NO (1900–1500 cm^{-1}) [60–63]. The characteristic peak at 2380–2315 cm^{-1} was confirmed as CO_2 [58,64]. CO was identified by the appearance of bands at 2180–2120 cm^{-1} [58,65]. The band at 3016 cm^{-1} represented CH_4 [66,67].

The important bands are enumerated in Table 2. From Figure 9, the asymmetric stretching vibrations of carbonyl (C=O) lead to the peak wavenumbers of 2350 cm^{-1} and 2345 cm^{-1}. A weak spectrum band at 1600–1450 cm^{-1} reveals the presence of an aromatic ring (skeleton stretching vibrations of aromatic ring C=C). The bands at 2200–2050 cm^{-1} (C-O stretch vibration) and 2480–2250 cm^{-1} (C=O stretch vibration) represent CO and CO_2, respectively. Moreover, the peak wavenumber of 3740 cm^{-1} indicates the release of H_2O. The bands of 3400–3100 cm^{-1} are owing to N-H stretching vibration, which indicated the presence of NH_3. The band at 3010 cm^{-1} corresponds to C-H stretching vibration, which leads to the formation of CH_4. In addition, the intensity of the absorption peak increases with the increase in temperature. The release of CH_4 is related to the pyrolysis of the benzene ring of coal. The amount of CH_4 produced at 600 °C is much greater than the other two temperatures, which indicates the macromolecular structure of coal was seriously damaged at 600 °C. The release of gas products at higher temperatures may come from the pyrolysis of aromatic carbon.

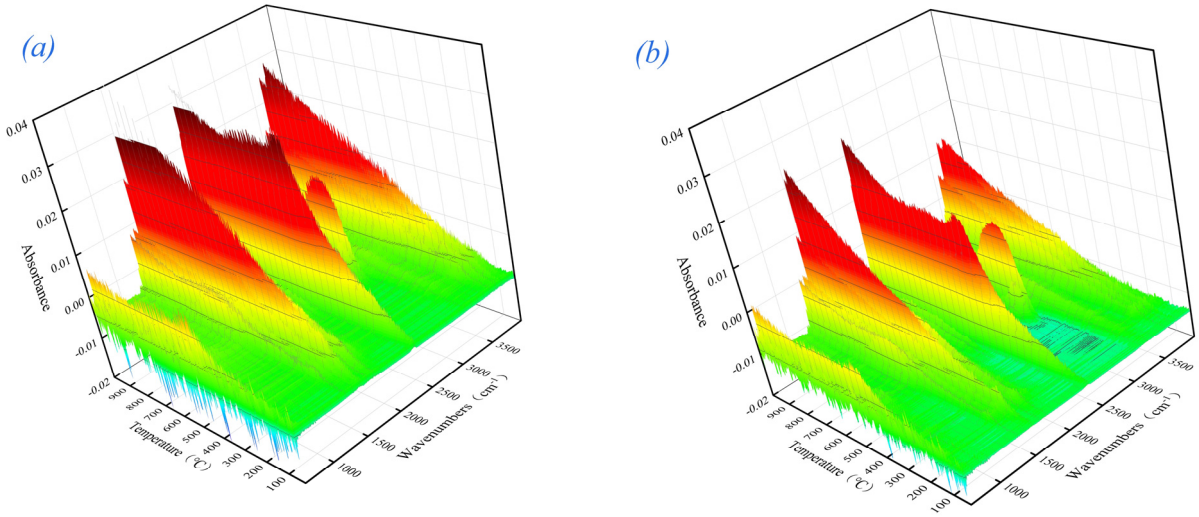

Figure 8. Three-dimensional infrared spectra of coal samples ((**a**): infrared spectra of SGT-1, (**b**): infrared spectra of SGT-4).

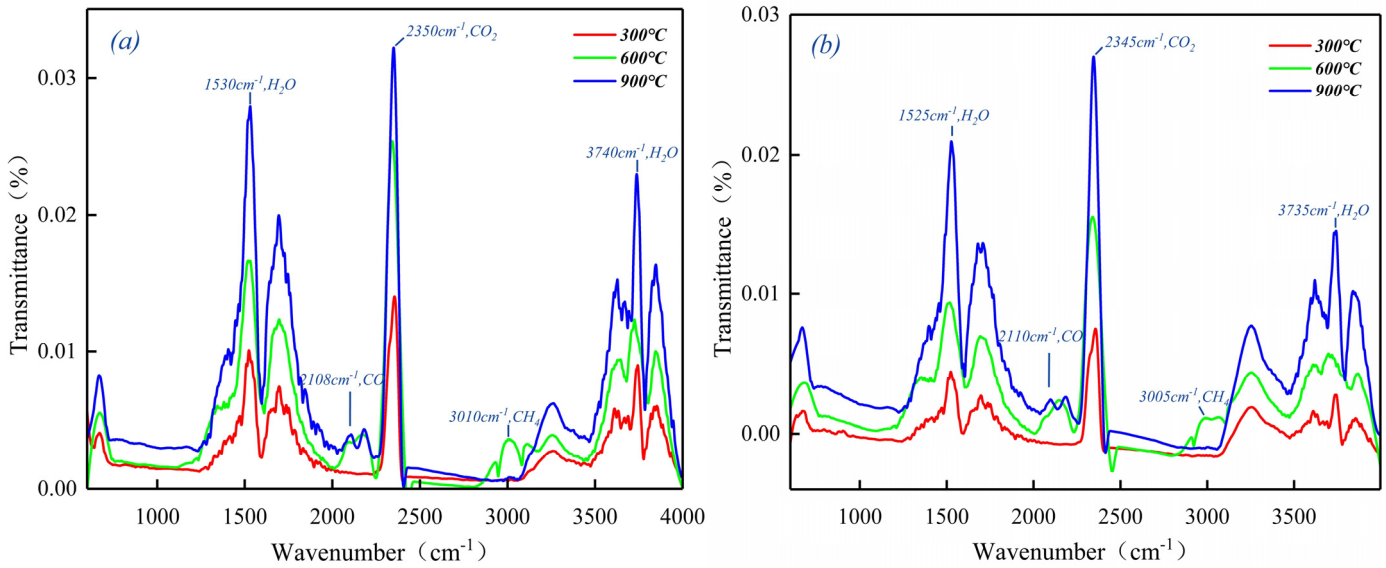

Figure 9. Two-dimensional infrared spectra of volatile products at different temperatures during the pyrolysis of coal samples ((**a**): infrared spectra of volatile products of SGT-1, (**b**): infrared spectra of volatile products of SGT-4).

Table 2. Gas species and functional groups characterized by the wavenumber range [68].

Detected Gas	Functional Group	Vibration	Wavenumber (cm^{-1})
H_2O	O-H	stretch	4000–3500
	H-O-H	bending	1875–1275
CH_4	C-H	stretch	3000–2800
CO_2	C=O	stretch	2400–2240
	C=O	bending	736–605
CO	C-O	stretch	2240–2050
Aromatics	C=C and benzene skeleton	stretch	1690–1450
HCN	C-H	bending	815–615
NH_3	N-H	stretch	3340
	N-H	bending	966,927

2.4. The Catalytic Effect from the Inorganic Compounds

Figure 10 shows the relationship between ash content and maximum weight loss rate, which is negatively correlated. The decrease in ash content deepens the degree of pyrolysis products, which leads to gas products increasing in varying degrees. Ash content has an obvious impact on the generation of CH_4 and CO and a weak impact on the generation of H_2O and H_2, which is consistent with previous research results [69]. The influence of ash on coal pyrolysis mainly comes from the minerals in coal. Minerals can catalyze or inhibit coal pyrolysis.

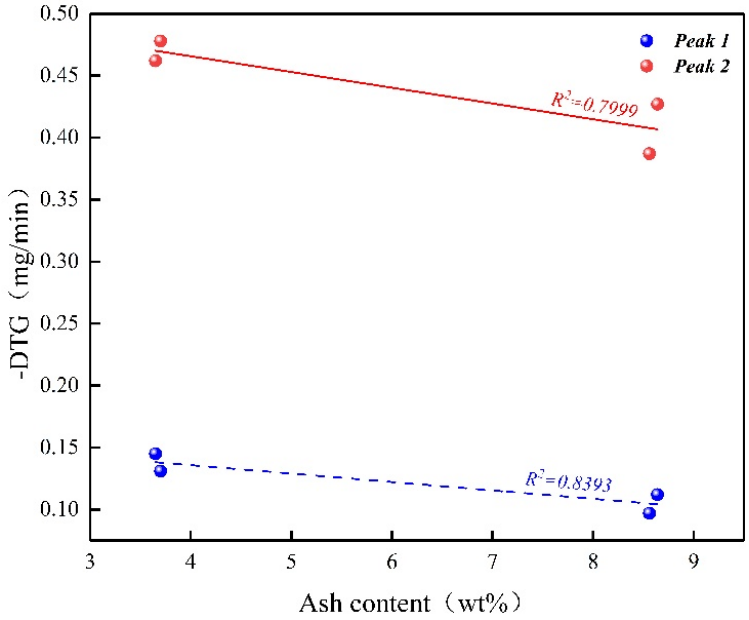

Figure 10. Relationship between ash content and maximum weight loss rate.

The mineral composition of the sample is shown in Table 2. It can be seen from Table 2 that SiO_2 and Al_2O_3 are the main minerals in the sample. At the same time, the component contents of alkali metals, alkaline earth metals, and iron oxides ($MgO + Fe_2O_3 + CaO + K_2O + Na_2O$) with carbon solution catalysis are very high, all above 25%. Therefore, we mainly discuss the effects of SiO_2, Al_2O_3, alkali metals, and alkaline earth metals on the pyrolysis of samples.

SiO_2 is an inert mineral with a high melting point. At the initial stage of the pyrolysis reaction, the chemical properties of SiO_2 will not change. With the progress of the reaction process, SiO_2 becomes the diluent in contact with the heated, softened particles of the tissue, which reduces the repolymerization reaction of coal tar macromolecules, and then generates more tar small molecules and gas-phase products, especially the formation of CO and H_2 in the later stage of the reaction (>800 °C). However, SiO_2 will not participate in the reaction of product formation and has no catalytic effect on the formation of gas-phase products. As the main material in clay minerals, Al_2O_3 has been widely recognized for its catalysis [31,70]. The catalytic reaction of Al_2O_3 on coal pyrolysis is mainly reflected in the high-temperature region, especially in dealkylation and dehydrogenation. However, due to the limitation of the experimental temperature, the catalytic effect of Al_2O_3 has not been well displayed.

Li et al. found that alkali metals and alkaline earth metals (AAEM) can inhibit the precipitation of large aromatic ring hydrocarbon compounds and then form solid products such as semicoke [71]. AAEM plays an important role in the fracture of old bonds and the formation of new bonds in the process of coal pyrolysis, especially the minerals connected with the organic structure of coal or semicoke. AAEM promotes the thermal decomposition of aliphatic hydrocarbons and small aromatic ring substances to produce

gas-phase products, but some studies believe that the internal minerals in coal have little effect on the pyrolysis activity of coal, and the effect on the yield of gas products can be ignored [72]. It can be seen from the above gas-phase product yield that the gas-phase product yield of SGT-3 and SGT-4 is significantly higher than that of SGT-1 and SGT-2. Therefore, AAEM inhibits the formation of tar and other products in the process of this pyrolysis, so that the precursor unit forming tar is repeatedly broken and bonded with the free radical in semicoke, Aliphatic fragments forming tar and some aromatic compounds with low molecular weight are precipitated in the form of gas.

2.5. The Mechanism for Thermal Pyrolysis of Tar-Rich Coal

According to the experimental results of TG-MS-FTIR in the argon atmosphere, the thermal pyrolysis characteristics of tar-rich coal under a nonoxidizing gaseous environment can be proposed. Firstly, the unstable bonds in the molecular structure of coal are removed with the increase in temperature, such as C-O-C and phenolic hydroxyl groups. The main gas generated in the low-temperature stage is H_2O because the water in the coal pores will escape with heating. Meanwhile, many small molecular products are formed at this stage. Secondly, the generation of volatiles increased with the increase in temperature. From the results of MS and FTIR data, volatiles are generated in large quantities after 400 °C, which means the cleavage of the benzene ring and small molecular structure. The cleavage of the aliphatic chain and aromatic chain is the source of CH_4 generation. H_2 is formed by the condensation of hydrogen radical formed by the cleavage of the aliphatic chain. The generation of CO is caused by the decomposition of alkyl and aromatic ether. The generation of CO_2 is related to oxygen-containing hybridization. In the high-temperature stage, the secondary cracking reaction reduces the yield of tar and increases the gaseous products. Due to the high tar yield of tar-rich coal, the yield of the volatile matter still increased after 900 °C.

3. Samples and Experimental Methods

3.1. Coal Samples

The experimental samples used in this work were from Shigetai Coal Mine, Shaanxi, China. This coal sample is typical tar-rich coal; there are high tar yields at low temperatures in samples. Four coal samples, Shigetai-1, Shigetai-2, Shigetai-3 and Shigetai-4 (SGT-1, SGT-2, SGT-3 and SGT-4), were used for this experiment. SGT-1 and SGT-2 were taken from one coal seam, SGT-3 and SGT-4 were taken from another coal seam. The coal samples had been placed in an air oven under 60 °C for 24 h to remove moisture. Then, the dried coal was crushed to a particle size below 80 mesh by a ball mill. Table 3 shows the results of the proximate and ultimate analysis of coal samples. Table 4 shows the ash composition analysis results of the samples. Proximate and ultimate analyses were carried out in the Testing Center of China National Administration Coal Geology (Xuzhou, China). C, H, O, N, S were determined following GB/T476-2008, GB/T19227-2008, and GB/T214-2007. Meanwhile, proximate analysis followed GB/T212-2008 and was used to detect moisture, volatile, ash, and fixed carbon. The analysis of ash composition was tested in the Testing Center of China National Administration Coal Geology (Xuzhou, China). Ash composition was determined following GB/T1574-2007. As shown in Table 2, the main components of coal ash are SiO_2, Al_2O_3, Fe_2O_3, and Cao. There are also small amounts of MgO, TiO_2, K_2O, Na_2O, P_2O_5, and SO_2.

Table 3. Proximate and ultimate analyses of coal samples.

	SGT-1	SGT-2	SGT-3	SGT-4
Ultimate analysis (wt %, daf)				
C_{daf}	75.91	76.03	76.45	76.33
H_{daf}	3.67	3.61	3.89	3.88
O_{daf}	18.40	18.50	18.15	18.31
N_{daf}	0.87	0.95	1.31	1.25
$S_{t,d}$	1.05	1.03	0.19	0.25
H/C	0.58	0.57	0.61	0.61
O/C	0.18	0.18	0.18	0.18
Proximate analysis (wt %)				
M_{ad}	13.40	13.45	14.72	14.82
A_d	8.64	8.56	3.65	3.70
V_{daf}	31.42	31.44	33.13	33.28
FC_d	62.66	62.61	64.43	64.56

($S_{t,d}$ is dry grade total sulfur; O_{daf} is dry ash-free oxygen; C_{daf} is dry ash-free carbon; H_{daf} is dry ash-free hydrogen; M_{ad} is moisture; A_d is dry ash-free ash; V_{daf} is dry ash-free volatile; F_{cd} is fixed carbon).

Table 4. The ash composition of coal samples.

Type	Composition Analysis of Ash (%)										
	K_2O	Na_2O	SiO_2	Al_2O_3	Fe_2O_3	CaO	MgO	SO_3	TiO_2	MnO_2	P_2O_5
SGT-1	0.25	0.69	41.09	18.06	12.62	11.16	1.20	12.12	0.82	0.083	0.020
SGT-2	0.27	0.75	40.95	18.01	12.65	11.16	1.25	12.05	0.85	0.082	0.021
SGT-3	0.24	3.12	33.31	13.12	15.61	17.34	3.21	11.80	0.55	0.125	0.032
SGT-4	0.23	3.11	33.31	13.07	15.60	17.33	3.11	11.70	0.57	0.127	0.032

3.2. TG/MS/FTIR Analyses

TG-MS-FTIR analyses were performed at the Institute of Coal Chemistry, Chinese Academy of Sciences (See the Figure S1). The experimental instrument consists of three parts: Thermogravimetry (SETARAM, Lyon, France), Mass spectrometry (PFEIFFER, Asslar, Germany), and Fourier transform infrared spectrometer (BRUKER, Ettlingen, Germany).

The thermal pyrolysis experiments were carried out in SETSYS EVOLUTION TGA 16/18 thermogravimetric analyzer. The dried samples were crushed below 200 mesh. About 20 mg sample was put into an alumina crucible and heated from 30 °C to 1000 °C at a heating rate of 10 °C/min under a high purity argon atmosphere with a gas flow of 50 mL/min. The thermal pyrolysis gas was detected by the mass spectrometer. According to previous studies, the most important gaseous products of coal pyrolysis are H_2O, CO_2, CO, H_2, and hydrocarbons [73,74]. The mass spectrometer has two functions: full scanning mode and selected ion recording (MID) mode. The former mode was used to detect the signals of all the fragment ions (m/z 1–160), and the latter mode tracked MS signals of some specific ions marked accurately as m/z 2, 16, 18, 28, 44. FTIR is a technique to characterize the chemical structure of coal, which is used to determine the functional group in coal [75–78]. By FTIR, the evolution of functional groups in coal during pyrolysis can be effectively detected. The wavelength ranges of the Fourier transform infrared spectrometer is from 4000 to 350 cm^{-1}.

4. Conclusions

In this work, efforts have been made to study the pyrolysis characteristics of two kinds of tar-rich coal through the TG-MS-FTIR. TG was used to detect the quality change of samples during pyrolysis. MS and FTIR were used to detect the evolution of gaseous products and functional groups, respectively. Moreover, the results measured by MS are compared with the data of FTIR analysis. As evidenced by the good consistency between

these two approaches, the result is reliable and accurate. Through the experimental results, the following conclusions are obtained:

During the pyrolysis process, the sample experienced two mass losses, the first was due to the loss of water in the sample, and the second mass loss was due to the formation of CO_2. The release of water and the depolymerization of macromolecules are the main reasons for the mass loss of samples.

The results of the MS and FTIR showed good consistency. The evolutions of gaseous compounds (i.e., H_2, H_2O, CO, CO_2, and CH_4) during pyrolysis could be measured by TG-MS-FTIR. The formation of gaseous compounds was related to the evolution of different functional groups in coal.

Ash content has a certain influence on coal pyrolysis. Specifically, the less ash, the more sufficient the coal pyrolysis reaction, which is caused by the minerals in coal. AAEM inhibited the formation of tar, promoted the pyrolysis of tar precursor products to form small molecular substances, and improved the yield of gas-phase products.

Based on the analysis of MS and FTIR data, the thermal pyrolysis characteristics of tar-rich coal are proposed.

Supplementary Materials: The following supporting information can be downloaded at: https://www.mdpi.com/article/10.3390/catal12040376/s1, Figure S1: The diagram of TG-MS-FTIR system.

Author Contributions: Data curation and writing—original draft preparation, Z.D.; supervision and writing—review and editing, W.L. All authors have read and agreed to the published version of the manuscript.

Funding: This research was funded by the National Natural Science Foundation of China, grant number 41972169.

Acknowledgments: We thank the National Natural Science Foundation of China (Grants No. 41972169).

Conflicts of Interest: The authors declare no conflict of interest.

References

1. Yang, H.; Ma, L. Study on distribution law and occurrence characteristics of rich oil in Zichang mining area. *World Sci. Res. J.* **2020**, *6*, 1–6.
2. Ju, Y.; Zhu, Y.; Zhou, H.; Ge, S.; Xie, H. Microwave pyrolysis and its applications to the in situ recovery and conversion of oil from tar-rich coal: An overview on fundamentals, methods, and challenges. *Energy Rep.* **2021**, *7*, 523–536. [CrossRef]
3. Wang, S.; Shi, Q.; Wang, S.; Shen, J.; Sun, Q.; Cai, Y. Resource property and exploitation concepts with green and low-carbon of tar-rich coal as coal-based oil and gas. *J. China Coal Soc.* **2021**, *46*, 1365–1377. (In Chinese)
4. Shen, J.; Wang, X.; Zhao, C.; Wang, S.; Guo, C.; Shi, Q.; Ma, W. Experimental study on multi-scale pore structure characteristics of tar-rich coal in Yushenfu mining area. *Coal Geol. Explor.* **2021**, *49*, 33–41. (In Chinese)
5. Han, D.; Yang, Q. *China Coalfield Geology*; China Coal Industry Publishing House: Beijing, China, 1979. (In Chinese)
6. Liu, L.; Gong, Z.; Wang, Z.; Zhang, H. Study on combustion and emission characteristics of chars from low-temperature and fast pyrolysis of coals with TG-MS. *Environ. Eng. Res.* **2020**, *25*, 522–528. [CrossRef]
7. Jayaraman, K.; Kök, M.; Gokalp, I. Thermogravimetric and mass spectrometric (TG-MS) analysis and kinetics of coal-biomass blends. *Renew. Energy* **2017**, *101*, 293–300. [CrossRef]
8. Vekemans, O.; Laviolette, J.; Chaouki, J. Co-combustion of coal and waste in pulverized coal boiler. *Energy* **2016**, *94*, 742–754. [CrossRef]
9. Jayaraman, K.; Kök, M.; Gokalp, I. Pyrolysis combustion and gasification studies of different sized coal particles using TGA-MS. *Appl. Therm. Eng.* **2017**, *125*, 1446–1455. [CrossRef]
10. Tromp, P.J.J. *Coal Pyrolysis*; Amsterdam University: Amsterdam, The Netherlands, 1987.
11. Wei, J.; Liu, X.; Guo, Q.; Chen, X.; Yu, G. A comparative study on pyrolysis reactivity and gas release characteristics of biomass and coal using TG-MS analysis. *Energy Sources Part A* **2018**, *40*, 1–7. [CrossRef]
12. Zhang, S.; Li, C.; Huang, R.; Xiao, Y.; Mao, R.; Huang, J.; Zhou, C. Thermogravimetric study of the kinetics and characteristics of the pyrolysis of pulverized coal. *Mater. Res. Express* **2020**, *7*, 085604.
13. He, C.; Tang, C.; Liu, W.; Dai, L.; Qiu, R. Co-pyrolysis of sewage sludge and hydrochar with coals: Pyrolytic behaviors and kinetics analysis using TG-FTIR and a discrete distributed activation energy model. *Energy Convers. Manag.* **2020**, *203*, 112226. [CrossRef]

14. Lin, Y.; Tian, Y.; Xia, Y.; Fang, S.; Liao, Y.; Yu, Z.; Ma, X. General distributed activation energy model (G-DAEM) on co-pyrolysis kinetics of bagasse and sewage sludge. *Bioresour. Technol.* **2019**, *273*, 545–555. [CrossRef] [PubMed]
15. Jiang, H.; Wang, M.; Li, Y.; Jin, L.; Hu, H. Integrated coal pyrolysis with steam reforming of propane to improve tar yield. *J. Anal. Appl. Pyrolysis* **2020**, *147*, 104805. [CrossRef]
16. Yao, Q.; Ma, M.; Liu, Y.; He, L.; Sun, M.; Ma, X. Pyrolysis characteristics of metal ion-exchanged Shendong coal and its char gasification performance. *J. Anal. Appl. Pyrolysis* **2021**, *155*, 105087. [CrossRef]
17. Li, Q.; Ye, H.; Wang, Z.; Zhou, H.; Wei, J. Characteristics and evolution of products under moderate and high temperature coal pyrolysis in drop tube furnace. *J. Energy Inst.* **2021**, *96*, 121–127. [CrossRef]
18. Jayaraman, K.; Kök, M.; Gokalp, I. Combustion mechanism and model free kinetics of different origin coal samples: Thermal analysis approach. *Energy* **2020**, *204*, 117905. [CrossRef]
19. Zhu, Y.; Wen, W.; Li, Y.; Lu, L.; Yang, J.; Xu, M.; Pan, Y. Pyrolysis study of Huainan coal with different particle sizes using TG analysis and online Py-PI-TOF MS. *J. Energy Inst.* **2020**, *93*, 405–414. [CrossRef]
20. Jeong, T.; Isworo, Y.; Jeon, C. Evaluation of Char Characteristics and Combustibility of Low-Rank-Coal Blends with Different Reflectance Distributions. *Energy Fuels* **2019**, *33*, 8014–8025. [CrossRef]
21. Yan, B.; Jiao, L.; Li, J.; Zhu, X.; Ahmed, S.; Chen, G. Investigation on microwave torrefaction: Parametric influence, TG-MS-FTIR analysis, and gasification performance. *Energy* **2021**, *220*, 119794. [CrossRef]
22. Ma, J.; Liu, J.; Jiang, X.; Shen, J. An improved parallel reaction model applied to coal pyrolysis. *Fuel Processing Technol.* **2021**, *211*, 106608. [CrossRef]
23. Pan, G. Characteristic Study of Some Different Kinds of Coal Particles Combustion with Online TG-MS-FTIR. *IOP Conf. Ser. Earth Environ. Sci.* **2018**, *111*, 012019. [CrossRef]
24. Wang, S.; Tang, Y.; Schobert, H.; Guo, Y.; Gao, W.; Lu, X. FTIR and simultaneous TG/MS/FTIR study of Late Permian coals from Southern China. *J. Anal. Appl. Pyrolysis* **2013**, *100*, 75–80. [CrossRef]
25. Pan, G. Characteristic Study of Shenmu Bituminous Coal Combustion with Online TG-MS-FTIR. *IOP Conf. Ser. Earth Environm. Sci.* **2018**, *111*, 012018. [CrossRef]
26. Wall, T. Mineral matter transformations and ash deposition in pulverised coal combustion. *Symp. Combust.* **1992**, *24*, 1119–1126. [CrossRef]
27. Burket, C.; Rajagopalan, R.; Foley, H. Overcoming the barrier to graphitization in a polymer-derived nanoporous carbon. *Carbon* **2008**, *46*, 501–510. [CrossRef]
28. Strydom, C.; Bunt, J.; Schobert, H.; Raghoo, M. Changes to the organic functional groups of an inertinite rich medium rank bituminous coal during acid treatment processes. *Fuel Process. Technol.* **2011**, *92*, 764–770. [CrossRef]
29. Dash, P.; Lingam, R.; Kumar, S.; Suresh, A.; Banerjee, P.; Ganguly, S. Effect of elevated temperature and pressure on the leaching characteristics of Indian coals. *Fuel* **2015**, *140*, 302–308. [CrossRef]
30. Cuest, A.; Dhamelincourt, P.; Laureyns, J.; Martinez-Alonso, A.; Tascon, J. Raman microprobe studies on carbon materials. *Carbon* **1994**, *32*, 1523–1532. [CrossRef]
31. Shao, J.; Rong, Y.; Chen, H.; Yang, H.; Lee, D. Catalytic effect of metal oxides on pyrolysis of sewage sludge. *Fuel Process. Technol.* **2010**, *91*, 1113–1118. [CrossRef]
32. Liu, Q.; Hu, H.; Zhou, Q.; Zhu, S.; Chen, G. Effect of inorganic matter on reactivity and kinetics of coal pyrolysis. *Fuel* **2004**, *83*, 713–718. [CrossRef]
33. Howard, D.; William, A.; Jack, B. Mineral matter effects on the rapid pyrolysis and hydropyrolysis of a bituminous coal: Effects of yields of char, tar, and light gaseous volatiles. *Fuel* **1981**, *61*, 155–160.
34. Ahmad, T.; Awan, I.; Nisar, J.; Ahmad, I. Influence of inherent minerals and pyrolysis temperature on the yield of pyrolysates of some Pakistani coals. *Energy Convers. Manag.* **2009**, *50*, 1163–1171. [CrossRef]
35. Sergey, V. Kinetic concepts of thermally stimulated reactions in solids: A view from a historical perspective. *Int. Rev. Phys. Chem.* **2000**, *19*, 45–60.
36. Arenillas, A.; Rubiera, F.; Pis, J.; Cuesta, M.; Iglesias, M.; Jimenez, A.; Suarez-Ruiz, I. Thermal behavior during the pyrolysis of low rank perhydrous coals. *J. Anal. Appl. Pyrolysis* **2003**, *68*, 371–385. [CrossRef]
37. Ofori, P.; Nguyen, A.V.; Firth, B.; Mcnally, C.; Hampton, M. The role of surface interaction forces and mixing in enhanced dewatering of coal preparation tailings. *Fuel* **2012**, *97*, 262–268. [CrossRef]
38. Shi, L.; Liu, Q.; Guo, X.; Wu, W.; Liu, Z. Pyrolysis behavior and bonding information of coal-A TGA study. *Fuel Process. Technol.* **2013**, *108*, 125–132. [CrossRef]
39. Zhang, L.; Xu, S.; Zhao, W.; Liu, S. Co-pyrolysis of biomass and coal in a free fall reactor. *Fuel* **2007**, *86*, 353–359. [CrossRef]
40. Wang, S.; Tang, Y.; Schobert, H.; Mitchell, G.; Liao, F.; Liu, Z. A thermal behavior study of Chinese coals with high hydrogen content. *Int. J. Coal Geol.* **2010**, *81*, 37–44. [CrossRef]
41. Zhang, D.; Liu, P.; Lu, X.; Wang, L.; Pan, T. Upgrading of low rank coal by hydrothermal treatment: Coal tar yield during pyrolysis. *Fuel Process. Technol.* **2016**, *141*, 117–122. [CrossRef]
42. Ding, L.; Zhou, Z.; Dai, Z.; Yu, G. Effects of coal drying on the pyrolysis and in-situ gasification characteristics of lignite coals. *Appl. Energy* **2015**, *155*, 660–670. [CrossRef]
43. Ahmed, I.; Gupta, A. Experiments and stochastic simulations of lignite coal during pyrolysis and gasification. *Appl. Energy* **2013**, *102*, 355–363. [CrossRef]

44. Hodek, W.; Kirschstein, J.; Heek, K. Reactions of oxygen containing structures in coal pyrolysis. *Fuel* **1991**, *70*, 424–428. [CrossRef]
45. Arenillas, A.; Rubiera, F.; Pis, J. Simultaneous thermogravimetric–mass spectrometric study on the pyrolysis behavior of different rank coals. *J. Anal. Appl. Pyrolysis* **1999**, *50*, 31–46. [CrossRef]
46. Metzinger, T.; Hüttinger, K. Investigations on the cross-linking of binder pitch matrix of carbon bodies with molecular oxygen —Part I. Chemistry of reactions between pitch and oxygen. *Carbon* **1997**, *35*, 885–892. [CrossRef]
47. Drbohlav, J.; Wtk, S. The oxidative stabilization and carbonization of a synthetic mesophase pitch, part II: The carbonization process. *Carbon* **1995**, *33*, 713–731. [CrossRef]
48. Garcia, R.; Arenillas, A.; Crespo, J.; Pis, J.; Moinelo, S. A Comparative TG-MS Study of the Carbonization Behavior of Different Pitches. *Energy Fuels* **2002**, *16*, 935–943. [CrossRef]
49. Chen, H.; Li, B.; Zhang, B. Effects of mineral matter on products and sulfur distributions in hydropyrolysis. *Fuel* **1999**, *78*, 713–719. [CrossRef]
50. Heek, K.; Hodek, W. Structure and pyrolysis behavior of different coals and relevant model substances. *Fuel* **1994**, *73*, 886–896. [CrossRef]
51. Zheng, L.; Furimsky, E. Assessment of coal combustion in O_2 + CO_2 by equilibrium calculations. *Fuel Process. Technol.* **2003**, *81*, 23–34. [CrossRef]
52. Glarborg, P.; Bentzen, L. Chemical Effects of a High CO_2 Concentration in Oxy-Fuel Combustion of Methane. *Energy Fuels* **2008**, *22*, 291–296. [CrossRef]
53. Strugnell, B.; Patrick, J. Rapid hydropyrolysis studies on coal and maceral concentrates. *Fuel* **1996**, *75*, 183. [CrossRef]
54. Bai, J.; Chen, X.; Shao, J.; Jia, C.; Wang, Q. Study of breakage of main covalent bonds during co-pyrolysis of oil shale and alkaline lignin by TG-FTIR integrated analysis. *J. Energy Inst.* **2019**, *92*, 512–522. [CrossRef]
55. Yan, M.; Bai, Y.; Li, S.; Lin, H.; Yan, D.; Shu, C. Factors influencing the gas adsorption thermodynamic characteristics of low-rank coal. *Fuel* **2019**, *248*, 117–126. [CrossRef]
56. Reichel, D.; Siegl, S.; Neubert, C.; Krzack, S. Determination of pyrolysis behavior of brown coal in a pressurized drop tube reactor. *Fuel* **2015**, *158*, 983–998. [CrossRef]
57. Luo, L.; Liu, J.; Zhang, H.; Ma, J.; Wang, X.; Jiang, X. TG-MS-FTIR study on pyrolysis behavior of superfine pulverized coal. *J. Anal. Appl. Pyrolysis* **2017**, *128*, 67–74. [CrossRef]
58. Xu, T.; Huang, X. Study on combustion mechanism of asphalt binder by using TG–FTIR technique. *Fuel* **2010**, *89*, 2185–2190. [CrossRef]
59. Opata, Y.; Grivel, J. Synthesis and thermal decomposition study of dysprosium trifluoroacetate. *J. Anal. Appl. Pyrolysis* **2018**, *132*, S1035497363. [CrossRef]
60. Scaccia, S. TG–FTIR and kinetics of devolatilization of Sulcis coal. *J. Anal. Appl. Pyrolysis* **2013**, *104*, 95–102. [CrossRef]
61. Ahamad, T.; Alshehri, S. TG–FTIR–MS (Evolved Gas Analysis) of bidi tobacco powder during combustion and pyrolysis. *J. Hazard. Mater.* **2012**, *199*, 200–208. [CrossRef]
62. Wang, Z.; Lv, P.; Yuan, H.; Hu, K. Thermal degradation study of intumescent flame retardants by TG and FTIR: Melamine phosphate and its mixture with pentaerythritol. *J. Anal. Appl. Pyrolysis* **2009**, *86*, 207–214. [CrossRef]
63. Li, X.; Chen, L.; Dai, X.; Mei, Q.; Ding, G. Thermogravimetry–Fourier transform infrared spectrometry–mass spectrometry technique to evaluate the effect of anaerobic digestion on gaseous products of sewage sludge sequential pyrolysis. *J. Anal. Appl. Pyrolysis* **2017**, *126*, 288–297. [CrossRef]
64. Brebu, M.; Tamminen, T.; Spiridon, I. Thermal degradation of various lignins by TG-MS/FTIR and Py-GC-MS. *J. Anal. Appl. Pyrolysis* **2013**, *104*, 531–539. [CrossRef]
65. Yang, J.; Chen, H.; Zhao, W.; Zhou, J. TG-FTIR-MS study of pyrolysis products evolving from peat. *J. Anal. Appl. Pyrolysis* **2016**, *117*, 296–309. [CrossRef]
66. Weng, J.; Liu, Y.; Zhu, Y.; Pan, Y.; Tian, Z. Online study on the co-pyrolysis of coal and corn with vacuum ultraviolet photoionization mass spectrometry. *Bioresour. Technol.* **2017**, *244*, 125–131. [CrossRef]
67. Huang, Y.; Liu, H.; Yuan, H.; Zhuang, X.; Yuan, S.; Yin, X.; Wu, C. Association of chemical structure and thermal degradation of lignins from crop straw and softwood. *J. Anal. Appl. Pyrolysis* **2018**, *134*, 25–34. [CrossRef]
68. Liang, B.; Wang, J.; Hu, J.; Li, C.; Li, R.; Liu, Y.; Zeng, K.; Yang, G. TG-MS-FTIR study on pyrolysis behavior of phthalonitrile resin. *Polymer Degradat. Stabil.* **2019**, *169*, 108954. [CrossRef]
69. Chen, X.; Chen, Y.; Yang, H.; Chen, W.; Wang, X.; Chen, H. Fast pyrolysis of cotton stalk biomass using calcium oxide. *Bioresour. Technol.* **2017**, *233*, 15–20. [CrossRef]
70. Sun, Y.; Chen, J.; Zhang, Z. General roles of sludge ash, CaO and Al_2O_3 on the sludge pyrolysis toward clean utilizations. *Appl. Energy* **2019**, *233*, 412–423. [CrossRef]
71. Li, C.; Sathe, C.; Kershaw, J.; Pang, Y. Fates and roles of alkali and alkaline earth metals during the pyrolysis of a Victorian brown coal. *Fuel* **2000**, *79*, 427–438. [CrossRef]
72. Wang, M.; Fu, C.; Chang, L.; Xie, K. Effect of fractional step acid treatment process on the structure and pyrolysis characteristics of Ximeng brown coal. *J. Fuel Chem. Technol.* **2012**, *40*, 906–911.
73. Wang, W. Chemical reactions in thermal decomposition of coal. *Fuel Process. Technol.* **1988**, *20*, 317–336.
74. Solomon, P.; Serio, M.; Suuberg, E. Coal pyrolysis: Experiments, kinetic rates and mechanisms. *Progress Energy Combust. Sci.* **1992**, *18*, 133–220. [CrossRef]

75. Painter, P. Fourier transform infrared study of acid-demineralized coal. *Fuel* **1978**, *57*, 125–126. [CrossRef]
76. Painter, P.; Coleman, M.; Jenkins, R.; Whang, P.; Walker, J. Fourier transform infrared study of mineral matter in coal. A novel method for quantitative mineralogical analysis. *Fuel* **1978**, *57*, 337–344. [CrossRef]
77. Painter, P.; Snyder, R.; Starsinic, M.; Coleman, M.; Kuehn, D.; Davis, A. Concerning the application of FT-IR to the study of coal: A critical assessment of band assignments and the application of spectral analysis programs. *Appl. Spectrosc.* **1981**, *35*, 475–485. [CrossRef]
78. Geng, W.; Nakajima, T.; Takanashi, H.; Ohki, A. Analysis of carboxyl group in coal and coal aromaticity by fourier transform infrared (FT-IR) spectrometry. *Fuel* **2009**, *88*, 139–144. [CrossRef]